# The matter spectral density from lensed CMB observations.

Ethan Anderes and Alexander van Engelen

**Abstract** We use local likelihood estimates of gravitational shear and convergence from lensed cosmic microwave background observations to estimate the projected mass spectral density. Typically there is an additive bias when using a plug-in estimate of the spectral density from a noisy estimate of the random field. We explore the possibility of adjusting this bias by subtracting an approximate power spectrum of the noise in the reconstruction using unlensed simulations. We demonstrate some empirical results that suggest the remaining biases complement those seen in the quadratic estimate developed by Hu and Okamoto [9, 10, 16]. We finish the paper with a discussion regarding the potential scientific applications and the challenges associated with estimating the noise spectrum from simulations.

## 1 Introduction

Over the past decade the cosmic microwave background (CMB) has emerged as a fundamental probe of cosmology and astrophysics. In addition to the primary fluctuations of the early Universe, the CMB contains signatures of the gravitational bending of CMB photon trajectories due to matter, called gravitational lensing. Mapping this gravitational lensing is important for a number of reasons including, but not limited to, understanding cosmic structure, constraining cosmological parameters [12, 18] and detecting gravitational waves [14, 13, 17]. In this paper we investigate the possibility of using simulations to correct a bias when using a plug-in estimate of the matter spectral density from local likelihood estimates of gravitational lensing.

Two estimates have emerged for reconstructing the gravitational potential: the quadratic estimator (developed in [9, 10, 16]) and a global maximum likelihood es-

Ethan Anderes
University of California, Davis, CA 95616, e-mail: anderes@stat.ucdavis.edu

Alexander van Engelen
McGill University, Montréal H3A 2T8, e-mail: engelen@physics.mcgill.ca

timate (developed in [6, 7]). The quadratic estimator, which is arguably the most popular, uses a first order Taylor approximation to establish mode coupling in the Fourier domain which can be estimated to recover the gravitational potential (real space analogs to these estimators can be found in [2, 3]). The maximum likelihood estimate, on the other hand, uses likelihood approximations to find an MLE for estimating the lensing potential. A new estimate developed in [1] uses a local Bayesian approach that avoids the computational difficulties associated with a full scale likelihood approach. This approach estimates the local curvature of the gravitational potential on sliding local neighborhoods of the observed CMB temperature and polarization fields. A low pass filter of the true gravitational potential is then constructed by stitching together local curvature estimates. The local analysis allows one to avoid using the typical first order Taylor expansion for the quadratic estimator and avoids the likelihood approximations used in global estimates. Moreover, the likelihood is computed in position space and therefore can easily deal with point source foregrounds, masking, nonstationary noise and nonstationary beams.

In [1] the local Bayesian method is shown to accurately reconstruct the gravitational potential under nearly ideal experimental conditions when observing both the temperature and the polarization field. In this paper, we consider the temperature fluctuations only. For more realistic experimental conditions the estimated projected mass can be noisy, especially at high frequency. However, using the isotropic assumption one can radially average the squared modulus of the Fourier transform of the estimate to approximate the spectral density. In doing so, one potentially gets accurate estimates of the mass spectral density even with small signal-to-noise ratios at each individual frequency of the mapping estimate.

There are two difficulties that arise when using locally estimated maps to estimate the spectral density. First, the observational noise weakens the amount of local information for gravitational shear and convergence. This has the impact of shrinking the local Bayes estimates toward the prior mean (at zero). The alternative, a local MLE estimate, is not as regularized and can have large estimation noise in the presence of weak local information. Using either of these estimates for estimating the spectral density yields significant biases: high bias for local MLE and low bias for local Bayes. In FIG. 1 we show the plug-in estimates of spectral density using the local MLE and Bayes estimates from one simulation of a lensed temperature field on a $10^{\text{o}} \times 10^{\text{o}}$ patch of the flat sky observed on 1 arcmin pixels with 2-$\mu K$ noise and beam FWHM of 4 arcmin. The dashed line with stars shows the plug-in estimate from the local Bayes technique, which is clearly shrunk toward zero. The dashed line with triangles shows the local MLE technique, which has a high bias from the estimation error.

In an attempt to mitigate these biases we work with the overly noisy MLE estimate but correct the resulting bias in the plug-in spectral density estimate using simulations. The dashed line with circles in FIG. 1 shows this new estimate. It is clear that this technique has significantly less bias than either the local MLE or the Bayes estimate. However, to make this new technique scientifically useful one needs a theoretical understanding of the behavior of the local MLE estimate in both the lensed and unlensed case (since unlensed simulations are used to correct the bias).

There are two main difficulties in deriving such an understanding. First, the estimates are implicitly defined as a maximizer of the local likelihood and, as such, there is no closed form. Secondly, the typical asymptotic arguments used for MLE estimates hold as the signal-to-noise ratio approaches infinity. Since the signal-to-noise ratio is very low on each local neighborhood one might expect the estimates to behave differently than their asymptotic cousins.

The remainder of the paper is organized as follows. In Section 2 we give a detailed account of the local MLE and Bayesian estimates. Then in Section 3 we discuss how estimation error propagates to biases in plug-in estimates of spectral density and how to estimate the bias with simulations. We present numerical evidence that one can subtract this estimated bias to produce estimates of spectral density that are comparable to the quadratic estimator found in the current literature. Finally, in Section 5, we discuss the challenges associated with local estimates of lensing and the resulting estimates of spectral density. We emphasize that the goal of this paper is to partly give some hints at the success of a new method but primarily to illuminate the challenges associated with local likelihood estimates in general.

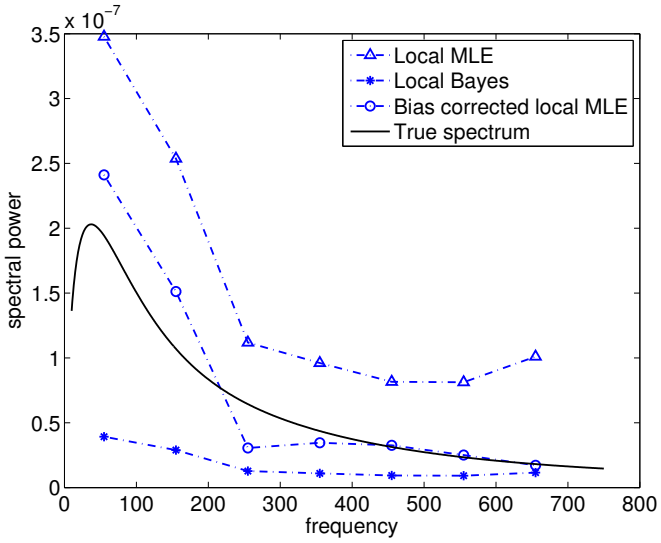


**Fig. 1** Solid line shows the input theoretical spectrum; triangles show a local MLE estimate of the spectrum; stars show the local Bayes estimate of the spectrum; circles show the bias corrected local MLE estimate of spectral density. The simulation is on a $10^o \times 10^o$ patch of the flat sky observed on 1 arcmin pixels with 2-$\mu K$ noise and beam FWHM of 4 arcmin.

## 2 Local estimates of shear and convergence

The CMB radiation measures temperature fluctuations of the early Universe some 400,000 years after the big bang. Let $T(\boldsymbol{x})$ denote these fluctuations (measured in units $\mu K$) on the observable sky. In this paper we work with the small angle limit and use a flat sky approximation so that $\boldsymbol{x} \in \mathbb{R}^2$. Instead of directly observing $T$ we observe a remapping of the CMB due to the gravitational effect of intervening matter. This lensed CMB can be written $T(\boldsymbol{x}+\nabla\phi(\boldsymbol{x}))$ where $\phi$ denotes the gravitational potential (see [4], for example).

To describe the local estimate of $\phi$ from the lensed CMB, developed in [1], first consider a small circular observation patch with diameter $\delta$ in the flat sky centered at some point $\boldsymbol{x}_0$, denoted $\mathscr{N}_\delta(\boldsymbol{x}_0) \subset \mathbb{R}^2$. Over this small region we decompose $\phi$ into an overall local quadratic $q^\phi$ and error term $\varepsilon$ so that

$$\phi = q^\phi + \varepsilon.$$

The global estimate of $\phi$ is based on stitching together local estimates of $q^\phi$, denoted $\hat{q}^\phi$, from the lensed CMB observed on $\mathscr{N}_\delta(\boldsymbol{x}_0)$. Notice that as $\delta \to 0$ the expected magnitude of the error $\varepsilon$ approaches zero. This has the effect of improving the following Taylor approximation

$$T(\boldsymbol{x}+\nabla\phi(\boldsymbol{x})) = T(\tilde{\boldsymbol{x}}) + \nabla\varepsilon(\boldsymbol{x}) \cdot \nabla T(\tilde{\boldsymbol{x}}) + \cdots \tag{1}$$

for $\boldsymbol{x} \in \mathscr{N}_\delta(\boldsymbol{x}_0)$, where we use the notation $\tilde{\boldsymbol{x}} \equiv \boldsymbol{x} + \nabla q^\phi(\boldsymbol{x})$. Notice that $\tilde{\boldsymbol{x}}$ depends not only on $\boldsymbol{x}$ but also the unknown coefficients of the quadratic term $q^\phi$. Now when $\delta$ is sufficiently small we can truncate the expansion in (1) to get

$$T(\boldsymbol{x}+\nabla\phi(\boldsymbol{x})) \approx T(\boldsymbol{x}+\nabla q^\phi(\boldsymbol{x})) \tag{2}$$

on the local neighborhood $\mathscr{N}_\delta(\boldsymbol{x}_0)$. By regarding $q^\phi$ as unknown we can use the right hand side of (2) to develop a likelihood for estimating the coefficients of $q^\phi$. Nominally $q^\phi$ has 6 unknown coefficients for which to estimate. However, we can ignore the linear terms in $q^\phi$ since the CMB temperature and the polarization are statistically invariant under the resulting translation in $\nabla q^\phi$. Therefore, one can write $q^\phi$ as $c_1(x-x_0)^2/2 + c_2(x-x_0)(y-y_0) + c_3(y-y_0)^2/2$ for unknown coefficients $c_1 = q^\phi_{xx}, c_2 = q^\phi_{xy}, c_3 = q^\phi_{yy}$.

### *2.1 The local likelihood*

Using the Gaussian approximation of the CMB along with the quadratic potential approximation given by (2) one can construct the likelihood as a function of the unknown quadratic coefficients in $q^\phi$. Let $\boldsymbol{x}_1, \ldots, \boldsymbol{x}_n$ denote the observation locations of the CMB within the local neighborhood $\mathscr{N}_\delta(\boldsymbol{x}_0)$ centered at $\boldsymbol{x}_0$. Using approxi-

mation (2), the CMB observables in this local neighborhood are well modeled by white noise corruption of a convolved (by the beam) lensed intensity field $T$. Let $\boldsymbol{t}$ denote the $n$-vector of observed CMB values at the corresponding pixel locations in $\mathscr{N}_\delta(\boldsymbol{x}_0)$ for the intensity $T$. Let $\varphi$ denote the instrumental beam so that the $k^{\text{th}}$ entry of $\boldsymbol{t}$ is modeled as

$$t_k \approx \int_{\mathbb{R}^2} d^2\boldsymbol{x}\, \varphi(\boldsymbol{x}) T(\tilde{\boldsymbol{x}}_k - \tilde{\boldsymbol{x}}) + \sigma_T n_k \tag{3}$$

where the $n_k$'s are independent standard Gaussian random variables, $\tilde{\boldsymbol{x}}_k = \boldsymbol{x}_k + \nabla q^\phi(\boldsymbol{x}_k)$ and $\tilde{\boldsymbol{x}} = \boldsymbol{x} + \nabla q^\phi(\boldsymbol{x})$. Note that this is an approximate model for $t_k$ based on (2). In actuality, the $k^{\text{th}}$ temperature measurement is $\int_{\mathbb{R}^2} d^2\boldsymbol{x}\, \varphi(\boldsymbol{x}) T(\boldsymbol{x}_k - \boldsymbol{x} + \nabla\phi(\boldsymbol{x}_k - \boldsymbol{x})) + \sigma_T n_k$, but the linearity of $\nabla q^\phi$ allows us to write $\boldsymbol{x}_k - \boldsymbol{x} + \nabla\phi(\boldsymbol{x}_k - \boldsymbol{x}) \approx \textit{constant} + \tilde{\boldsymbol{x}}_k - \tilde{\boldsymbol{x}}$ on the small neighborhood $\mathscr{N}_\delta(\boldsymbol{x}_0)$. Since one can write $\boldsymbol{x} + \nabla q^\phi(\boldsymbol{x}) = M\boldsymbol{x}$ where the $M$ is a $2\times 2$ real matrix, the sheared temperature $T(\tilde{\boldsymbol{x}})$ is a stationary random field with spectral density given by $C^{TT}_{M^{-1}\boldsymbol{\ell}} \det M^{-1}$. After adjusting for the beam (which is applied after lensing) the covariance between the observations in $\boldsymbol{t}$ can be written

$$\left\langle t_k t_j \right\rangle_{\text{T}} \approx \sigma_T^2 \delta_{ij} + \int_{\mathbb{R}^2} \frac{d^2\boldsymbol{\ell}}{(2\pi)^2} e^{i\boldsymbol{\ell}\cdot(\boldsymbol{x}_k - \boldsymbol{x}_j)} |\varphi(\boldsymbol{\ell})|^2 \frac{C^{TT}_{M^{-1}\boldsymbol{\ell}}}{\det M}. \tag{4}$$

*Remark:* We use the notation $\langle\cdot\rangle_{\text{T}}$ to denote expectation, or ensemble average, with respect to both the CMB temperature field $T(\boldsymbol{x})$ and the observational noise $n_k$. Conversely, we use the notation $\langle\cdot\rangle_\phi$ to denote expectation with respect to the large scale structure $\phi$ and for brevity we write $\langle\cdot\rangle \equiv \langle\langle\cdot\rangle_{\text{T}}\rangle_\phi$ where the expectations are done under the assumption that $T$ and $\phi$ are independent.

Now, using Gaussianity of the full vector of CMB observables the log likelihood (up to a constant), as a function of the quadratic fit $q^\phi$, can be written

$$\mathscr{L}(q^\phi|\boldsymbol{t}) = -\frac{1}{2}\boldsymbol{t}^\dagger \left(\Sigma_{q^\phi} + \sigma_T^2 I\right)^{-1} \boldsymbol{t} - \frac{1}{2}\ln\det\left(\Sigma_{q^\phi} + \sigma_T^2 I\right) \tag{5}$$

where $\Sigma_{q^\phi} + \sigma_T^2 I$ is the covariance matrix of the observation vector $\boldsymbol{t}$ containing the covariances $\left\langle t_k t_j \right\rangle_{\text{T}}$ given in (4) and $\sigma_T^2 I$ is the noise covariance structure where $I$ is the $n\times n$ identity matrix. Notice that the noise structure does not depend on the unknown quadratic $q^\phi$. In addition, one can utilize a single FFT to quickly compute the integral (4) for sufficient resolution in the argument $\boldsymbol{x}_k - \boldsymbol{x}_j$ to recover $\left\langle t_k t_j \right\rangle_{\text{T}}$ for all pairs $k, j$.

## *2.2 The local posterior*

In [1] it is argued that the local estimates of $q^\phi$ are modeled by a lowpass filter of the true gravitational potential. In particular, the quadratic function $q^\phi$ can be modeled by

$$q^{\phi}(\boldsymbol{x}) \approx \int \frac{d^2\boldsymbol{\ell}}{2\pi} e^{i\boldsymbol{x}\cdot\boldsymbol{\ell}} \phi^{\mathrm{lp}}(\boldsymbol{\ell})$$

over $\boldsymbol{x} \in \mathscr{N}_{\delta}(\boldsymbol{x}_0)$, where $\phi^{\mathrm{lp}}(\boldsymbol{\ell}) \equiv \varphi_{\delta}(\boldsymbol{\ell})\phi(\boldsymbol{\ell})$, with low-pass filter defined by

$$\varphi_{\delta}(\boldsymbol{\ell}) \approx \min\Big\{1, \Big[2 - \frac{\delta}{\pi}|\boldsymbol{\ell}|\Big]^{+}\Big\}. \tag{6}$$

Therefore a natural candidate for the prior on the coefficients of $q^{\phi}$ is the distribution of the random variables $\frac{\partial^2 \phi^{\mathrm{lp}}(0)}{\partial x_k \partial x_j}$. These are mean zero and Gaussian with variances obtained by the corresponding spectral moments of $\phi^{\mathrm{lp}}$. Letting this prior be denoted by $\pi(q^{\phi})$ the posterior distribution on $q^{\phi}$, which we maximize to estimate $q^{\phi}$ in the local Bayesian case, is

$$p(q^{\phi}|\boldsymbol{z}) \propto e^{\mathscr{L}(q^{\phi}|\boldsymbol{z})}\pi(q^{\phi}). \tag{7}$$

### *2.3 Stitching together the local curvatures*

The local MLE estimates of $q^{\phi}$ are found by maximizing (5) whereas the local Bayesian estimates are found by maximizing (7). These estimates give local quadratic fits to the true potential $\phi$, i.e. local curvature estimates: $\hat{\phi}^{\mathrm{lp}}_{xx}, \hat{\phi}^{\mathrm{lp}}_{xy}, \hat{\phi}^{\mathrm{lp}}_{yy}$. The global estimate of $\phi^{\mathrm{lp}}$ is found by stitching together these local the estimates. This is done in [1] by performing a gradient fit to $(\hat{\phi}^{\mathrm{lp}}_{xx}, \hat{\phi}^{\mathrm{lp}}_{xy})$ which gives $\hat{\phi}^{\mathrm{lp}}_{x}$ and a gradient fit to $(\phi^{\mathrm{lp}}_{xy}, \phi^{\mathrm{lp}}_{yy})$ which gives an estimate $\hat{\phi}^{\mathrm{lp}}_{y}$. A final gradient fit is then fit to the vector field $(\hat{\phi}^{\mathrm{lp}}_{x}, \hat{\phi}^{\mathrm{lp}}_{y})$ to obtain an estimate $\hat{\phi}^{\mathrm{lp}}$. The result of this iterated gradient fit is shown in FIG. 2 for a simulated lensed temperature field.

## 3 Spectral density estimates of projected mass

In this section we discuss the plug-in estimate of spectral density and show how estimation error propagates to biases in the spectral density estimate. We discuss this in the context of estimating the projected mass spectral mass density $C_{\ell}^{\kappa\kappa}$ where $\kappa$ denotes the convergence field (which is a tracer for mass fluctuations) and is defined by

$$\kappa \equiv -(\phi_{xx} + \phi_{yy})/2$$

using the shear notation given in [19]. The spectral density $C_{\ell}^{\kappa\kappa}$ is defined as the Fourier transform of the autocovariance function:

$$C_{\ell}^{\kappa\kappa} = \int d^2\boldsymbol{x}\, e^{-i\boldsymbol{\ell}\cdot\boldsymbol{x}} \langle \kappa(\boldsymbol{x})\kappa(\boldsymbol{0})\rangle_{\phi}.$$

Notice that $\langle \kappa(\boldsymbol{x})\kappa(\boldsymbol{0})\rangle_\phi$ gives the autocovariance since $\langle \kappa(\boldsymbol{x})\rangle_\phi = 0$.

To develop the estimate of $C_\ell^{\kappa\kappa}$ we need the following identity when $\kappa$:

$$\langle \kappa(\boldsymbol{\ell})\kappa(\boldsymbol{\ell}')^*\rangle_\phi = \delta_{\boldsymbol{\ell}-\boldsymbol{\ell}'} C_\ell^{\kappa\kappa}$$

This follows directly from the definition of spectral density, the assumption that $\kappa(\boldsymbol{x})$ is isotropic and the definition $\delta_{\boldsymbol{\ell}} \equiv \int \frac{d^2\boldsymbol{x}}{(2\pi)^2} e^{i\boldsymbol{x}\cdot\boldsymbol{\ell}}$. Notice that $\kappa(\boldsymbol{\ell})$ is technically a generalized process which behaves like $\sqrt{C_\ell^{\kappa\kappa}} W(\boldsymbol{\ell})$ where $W(\boldsymbol{\ell})$ is white noise. Therefore when working with finite sky observations of $\kappa(\boldsymbol{x})$ one can produce a discrete version of $\kappa(\boldsymbol{\ell})$ (using discrete Fourier transform) which satisfies $\left\langle |\kappa(\boldsymbol{\ell})|^2 \right\rangle_\phi \approx \frac{C_\ell^{\kappa\kappa}}{\Delta\boldsymbol{\ell}}$ where $\Delta\boldsymbol{\ell} \equiv \Delta\ell_1 \Delta\ell_2$ is the grid area in Fourier space. For the remainder of this paper we work with this discrete version of $\kappa$.

If one knew the convergence field $\kappa$ then one can estimate $C_\ell^{\kappa\kappa}$ by

$$\widehat{C_{\ell_0}^{\kappa\kappa}} = \frac{\Delta\boldsymbol{\ell}}{\#A_{\ell_0}} \sum_{\boldsymbol{\ell}\in A_{\ell_0}} \left|\kappa(\boldsymbol{\ell})\right|^2 \tag{8}$$

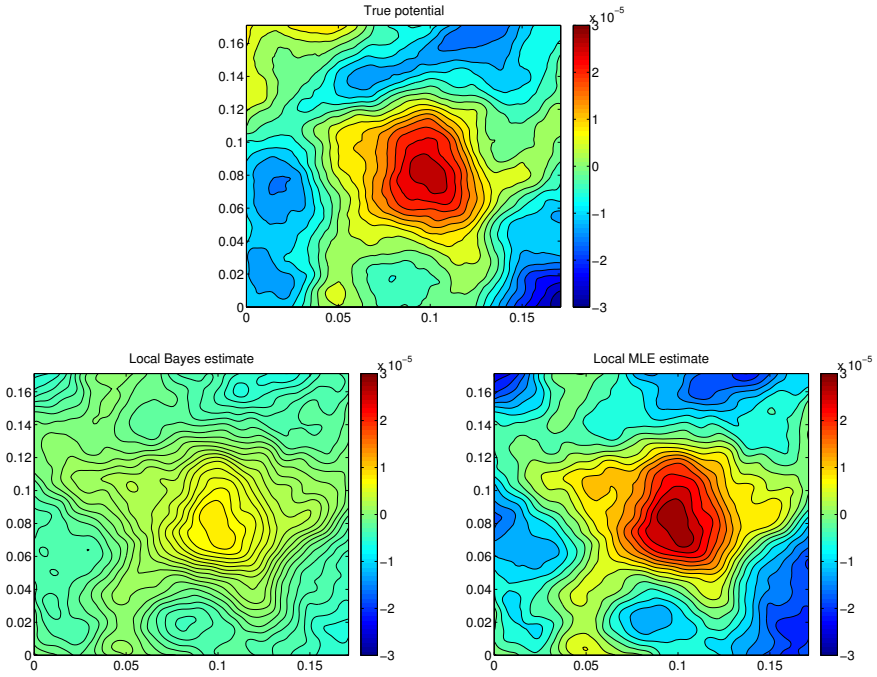


**Fig. 2** Estimated gravitational potential from simulated lensed CMB: input gravitational potential (top); local Bayes estimate (bottom left); local MLE estimate (bottom right). The lensed temperature simulation was observed on a $10^o \times 10^o$ patch of the flat sky with 1 arcmin pixels, 2-$\mu K$ noise and a beam FWHM of 4 arcmin.

where $\Delta\boldsymbol{\ell}$ denotes the area of the observation grid in $\boldsymbol{\ell}$; $A_{\ell_0}$ denotes a gridded annulus with radius $\ell_0$; $\#A_{\ell_0}$ denotes the number of grid points in $A_{\ell_0}$. Notice that this estimate is unbiased: $\langle \widehat{C_\ell^{\kappa\kappa}} \rangle_\phi = C_\ell^{\kappa\kappa}$.

In the case of the local MLE or Bayes estimates one has—$\hat{\phi}_{xx}^{\text{lp}}$, $\hat{\phi}_{yy}^{\text{lp}}$ and $\hat{\phi}_{xy}^{\text{lp}}$—the estimates of the mixed partial derivative as a function of local neighborhood midpoint. This leads to an estimate of $\kappa$ as

$$\hat{\kappa}(\boldsymbol{\ell}) \equiv -(\hat{\phi}_{xx}^{\text{lp}}(\boldsymbol{\ell}) + \hat{\phi}_{yy}^{\text{lp}}(\boldsymbol{\ell}))/(2\varphi_\delta(\boldsymbol{\ell}))$$

where $\varphi_\delta$ is the band pass filter, defined in (6), which approximates the local neighborhood effect discussed in [1]. One can then use $\hat{\kappa}$ to construct a plug-in estimate of $C_\ell^{\kappa\kappa}$ defined as

$$\widehat{C_{\ell_0}^{\hat{\kappa}\hat{\kappa}}} \equiv \text{“plug-in estimate”} = \frac{\Delta\boldsymbol{\ell}}{\#A_{\ell_0}} \sum_{\boldsymbol{\ell}\in A_{\ell_0}} \left|\hat{\kappa}(\boldsymbol{\ell})\right|^2. \tag{9}$$

The main problem with the plug-in estimate (9) is that estimation error from $\hat{\kappa}$ propagates to biases in $\widehat{C_\ell^{\hat{\kappa}\hat{\kappa}}}$. In the local Bayesian case, the estimation error results in a multiplicative shrinking bias as is seen in FIG. 1. Conversely there is a large additive bias for the local MLE plug-in estimate shown in FIG. 1. This bias has a simple explanation. If one lets $N$ denote the $\kappa$ estimation error (so that $\hat{\kappa} = \kappa + N$) then by assuming isotropy $\Delta\boldsymbol{\ell}\langle|\hat{\kappa}(\boldsymbol{\ell})|^2\rangle \approx C_\ell^{\kappa\kappa} + C_\ell^{\kappa N} + C_\ell^{N\kappa} + C_\ell^{NN}$ so that

$$\left\langle \widehat{C_\ell^{\hat{\kappa}\hat{\kappa}}} \right\rangle \approx C_\ell^{\kappa\kappa} + \underbrace{\left(C_\ell^{\kappa N} + C_\ell^{N\kappa} + C_\ell^{NN}\right)}_{\text{additive bias}} \tag{10}$$

where $C_\ell^{NN}$ is the spectrum for $N$ (assuming isotropy) and $C_\ell^{\kappa N}$ is the cross spectrum between $\kappa$ and $N$ so that $\langle \kappa(\boldsymbol{\ell}) N(\boldsymbol{\ell}')^* \rangle \equiv C_\ell^{\kappa N} \delta_{\boldsymbol{\ell}-\boldsymbol{\ell}'}$. For the local Bayes estimate the dominant source of bias is from the first two terms $C_\ell^{\kappa N} + C_\ell^{N\kappa}$ which is from the multiplicative shrinkage bias. Conversely, it seems the dominant source of bias for the local MLE estimate is from the last term, $C_\ell^{NN}$, which causes the upward bias seen in the dashed line with triangles in FIG. 1.

### *3.1 Bias correcting local MLE spectral estimates with simulations*

In the previous section we used $\hat{\phi}_{xx}^{\text{lp}}$, $\hat{\phi}_{yy}^{\text{lp}}$ and $\hat{\phi}_{xy}^{\text{lp}}$ to approximate the convergence $\kappa$ and construct the plug-in estimate $\widehat{C_\ell^{\hat{\kappa}\hat{\kappa}}}$. We argued that estimation error results in spectral density estimation bias which is quantified by $C_\ell^{\kappa N} + C_\ell^{N\kappa} + C_\ell^{NN}$. The two terms $C_\ell^{\kappa N} + C_\ell^{N\kappa}$ dominate the bias when using a local Bayesian estimate. Conversely, we will see that the dominant source of bias when using a local MLE estimate is from $C_\ell^{NN}$. The advantage of this scenario is that $C_\ell^{NN}$ has potential to be estimated using unlensed simulations (i.e. where $\kappa = 0$) whereas one must simulate

$\kappa$ under some fiducial model to approximate $C_\ell^{\kappa N} + C_\ell^{N\kappa}$. It is for this reason that we choose to use the noisy local MLE estimates, but correct the resulting bias in the plug-in spectral density estimate by approximating the noise spectrum $C_\ell^{NN}$ from unlensed simulations. In particular, we use the following bias-adjusted local MLE estimate of $C_\ell^{\kappa\kappa}$

$$\widehat{C_\ell^{\kappa\kappa}} \equiv \widehat{C_\ell^{\hat\kappa\hat\kappa}} - \widehat{C_\ell^{NN}} \tag{11}$$

where $\hat\kappa$ is the local MLE estimate of $\kappa$ and $\widehat{C_\ell^{NN}}$ is approximated using simulations. To construct $\widehat{C_\ell^{NN}}$ we use the local MLE estimation procedure for $\hat\kappa$ and run it on multiple realizations of unlensed CMB (with noise and beam) on the same pixel configuration of the observations. Since these simulations are done with $\kappa = 0$, the result is pure noise $N$. A spectral density estimate, based on $N$, is computed for each realization, which are then averaged over multiple realizations to construct $\widehat{C_\ell^{NN}}$.

*Remark:* In this paper we assume the noise spectrum is radially symmetric so that $\widehat{C_\ell^{NN}}$ is estimated by the same radial averaging as done in (9). If the beam or noise is asymmetric this assumption is unlikely to be true. However, one can still estimate the noise spectrum from simulations and subtract the resulting bias in $\widehat{C_\ell^{\hat\kappa\hat\kappa}}$.

## 4 Simulation

We use four types of simulations in this section, each summarized in Table 1. The lensed simulations (with additional noise and beam) are used to generate estimates of $\kappa$, using both the local MLE and quadratic estimates, which are then used to construct the plug-in estimates $\widehat{C_\ell^{\hat\kappa\hat\kappa}}$ given in Section 3. The unlensed simulations (also with additional noise and beam) are used to estimate the error spectrum, $\widehat{C_\ell^{NN}}$, derived in Section 3.1 for both the quadratic estimates and the local MLE estimates. We use periodic boundary conditions for the quadratic estimates to avoid complicated appodization issues inherent in the quadratic estimate based on non-periodic sky cuts. Due to computational time constraints only 35 simulations were made for the local MLE estimates (verses 100 simulations for the quadratic estimate).

The non-periodic lensed CMB fields are simulated[1] by generating a high resolution simulation of $T(\boldsymbol{x})$ and the gravitational potential $\phi(\boldsymbol{x})$ on a periodic $17^\circ \times 17^\circ$ patch of the flat sky with 0.25 arcmin pixels . The lensing operation is performed by taking the numerical gradient of $\phi$, then using linear interpolation to obtain the

[1] The fiducial cosmology used in our simulations is based on a flat, power law $\Lambda$CDM cosmological model, with baryon density $\Omega_b = 0.044$; cold dark matter density $\Omega_{\rm cdm} = 0.21$; cosmological constant density $\Omega_\Lambda = 0.74$; Hubble parameter $h = 0.71$ in units of $100\,{\rm km\,s^{-1}\,Mpc^{-1}}$; primordial scalar fluctuation amplitude $A_s(k = 0.002\,{\rm Mpc}^{-1}) = 2.45 \times 10^{-9}$; scalar spectral index $n_s(k = 0.002\,{\rm Mpc}^{-1}) = 0.96$; primordial helium abundance $Y_P = 0.24$; and reionization optical depth $\tau_r = 0.088$. The CAMB code is used to generate the theoretical power spectra [15].

**Table 1** The four types of simulations used to compare the bias adjusted local MLE and quadratic estimates of $C_\ell^{\kappa\kappa}$

| Simulation | Boundary type | Useage | Number of simulations |
|---|---|---|---|
| $T(\boldsymbol{x}+\nabla\phi(\boldsymbol{x}))$ | Periodic | $\widehat{C_\ell^{\hat\kappa\hat\kappa}}$ (using the quadratic estimate) | 100 |
| $T(\boldsymbol{x})$ | Periodic | $\widehat{C_\ell^{NN}}$ (using the quadratic estimate) | 100 |
| $T(\boldsymbol{x}+\nabla\phi(\boldsymbol{x}))$ | non-Periodic | $\widehat{C_\ell^{\hat\kappa\hat\kappa}}$ (using local MLEs) | 35 |
| $T(\boldsymbol{x})$ | non-Periodic | $\widehat{C_\ell^{NN}}$ (using local MLEs) | 35 |

lensed field $T(\boldsymbol{x}+\nabla\phi(\boldsymbol{x}))$. We down-sample the lensed field, every $4^{\text{th}}$ pixel, and restrict to a $10^{\text{o}} \times 10^{\text{o}}$ patch to obtain the desired arcmin pixel resolution for the simulation output. A Gaussian beam with a FWHM of 4 arcmin is applied in Fourier space using FFT of the lensed fields. Finally white noise is added in pixel space with a standard deviation of 2 $\mu K$-arcmin. A similar procedure is performed for the periodic lensed CMB fields, except the initial high resolution simulation of $T(\boldsymbol{x})$ and $\phi(\boldsymbol{x})$ are done on a periodic $10^{\text{o}} \times 10^{\text{o}}$ patch of the flat sky with 0.25 arcmin pixels.

The top plot of Fig. 3 summarizes the results using the local MLE estimates with a non-periodic cut sky. The bottom plot of Fig. 3 summarizes the corresponding results using the quadratic estimate on a periodic cut sky. Both show the ensemble average of the bias adjusted spectral density estimates $\widetilde{C_\ell^{\kappa\kappa}}$ (blue) compared to the true spectral density $C_\ell^{\kappa\kappa}$ (black) and the ensemble averaged spectrum $\widehat{C_\ell^{\kappa\kappa}}$ one would obtain if one had access to the true $\kappa$ field for each simulation (red). The bars denote standard deviation error bars. The reason we include $\widehat{C_\ell^{\kappa\kappa}}$ is to show the pixelization and appodization bias which is present irrespective of estimation procedure for $\kappa$.

Both estimates of $\widetilde{C_\ell^{\kappa\kappa}}$ based on the quadratic estimate and the local MLE estimate do a good job of tracking the true spectral density. It appears there is more variability in the local MLE estimate, especially at low $\ell$. However, at low $\ell$ the local MLE estimate looks nearly unbiased. The observed power suppression bias at low $\ell$ and power amplification bias at high $\ell$, for the quadratic estimator, is well documented in [5, 13]. It is interesting that the power amplification bias at high ell is opposite to the bias in the local MLE estimate. This may be due to a different Taylor truncation error used to derive the two different estimates. Irrespective of where the bias comes from, it is potentially scientifically useful that the biases are complementary.

*Note:* The ensemble averaged spectrum $\widehat{C_\ell^{\kappa\kappa}}$ based on the true $\kappa$ (red) is different at low $\ell$ in the top plot versus the bottom plot in Fig. 3. This is presumably do to the appodization effect which is present in the local MLE simulations, since we are using non-Periodic sky cuts, but not present for the period sky simulations used for the quadratic estimator.

## 5 Challenges

The main challenge for the local MLE procedure is the difficulty in deriving global properties of the noise structure. Since the local MLE estimate is based on a different Taylor truncation it may provide an important complement to the quadratic estimator. Indeed, the spectral density bias in the frequency range 300-600 seems entirely complimentary to the bias in the quadratic estimator. Moreover, the estimation variability also seems comparable in this range. However, the bias and variance most likely depends on the true, but unknown, spectrum $C_\ell^{\kappa\kappa}$. It remains to be seen if the bias remains complementary under alternative models for $C_\ell^{\kappa\kappa}$. Therefore, before it can be used in conjunction with the quadratic estimator, one must get some theoretical quantification of the nature of bias and variance.

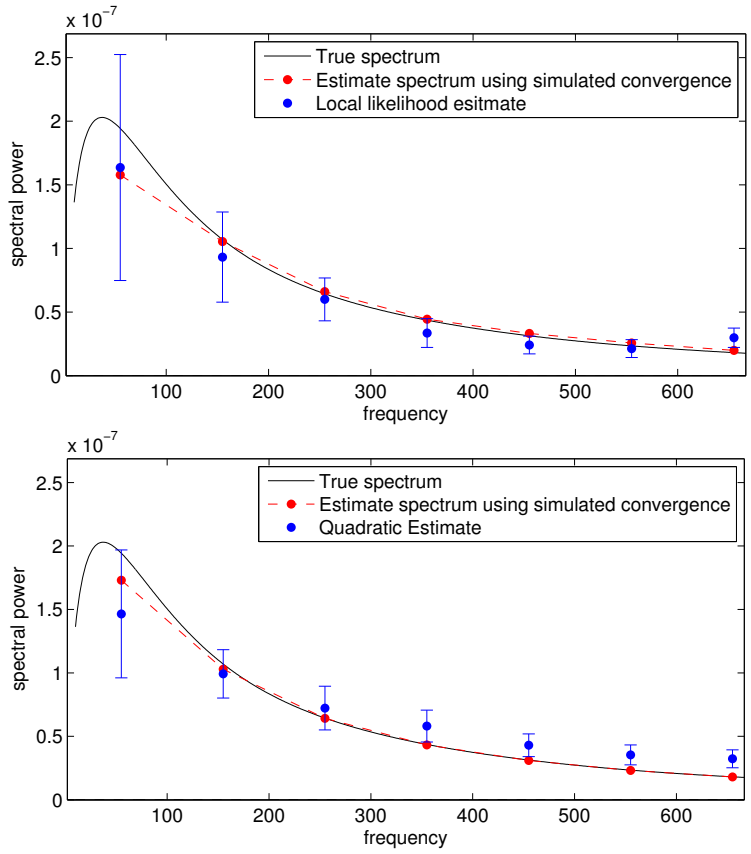


**Fig. 3** *Top:* The simulation results for the bias adjusted local MLE estimate of $C_\ell^{\kappa\kappa}$. The blue dots show the ensemble mean of the estimates ($1\sigma$ error bars). The red dots shows the mean of the estimates $\widehat{C_\ell^{\kappa\kappa}}$ if one had access to the true $\kappa$. *Bottom:* The corresponding results for the bias adjusted (with simulations) quadratic estimate of $C_\ell^{\kappa\kappa}$. See Section 4 for the simulation details.

It is clear from the results given in Section 4 that simulations can provide a partial answer to the quantification of bias and variance of the spectral density estimation. Unfortunately, the local MLE estimate is somewhat computationally expense. Each local estimate on a small neighborhood can be done quickly. However, these local estimates are required at a sufficient resolutions to get adequate coverage in Fourier space. Therefore a complete understanding of bias and variance seems unattainable through simulation.

One potential advantage of the local MLE estimate is the apparent unbiasedness at low $\ell$. This contrasts with the situation for the quadratic estimate, where the bias at low $\ell$ has been quantified by Hanson et. al. [5]. They present a method for correcting the low $\ell$ bias in the quadratic estimator. However, this method depends on a fiducial model for $C_\ell^{\kappa\kappa}$. Indeed, this problem persists when the quadratic estimator is applied to non-periodic sky cuts where quantification of the appodization effect is usually done with simulations under a fiducial model for $C_\ell^{\kappa\kappa}$. The advantage of the local MLE estimates, in this case, is that it does not require a fiducial model for first order bias correction or appodization. The cost of this unbiasedness, it seems, is the apparent increase in variability at low $\ell$.

**Acknowledgements** We thank Lloyd Knox for numerous helpful discussions.

## References

1. Anderes, E., Knox, L. & van Engelen, A., Phys, Rev D 83, 043523 (2011)
2. Bucher, M., Carvalho, C. S., Moodley, K., Remazeilles, M., arXiv:1004.3285 (2010)
3. Carvalho, C. S., Moodley, K., Phys. Rev. D 81, 123010 (2010)
4. Dodelson, S., *Modern cosmology*, Academic Press (2003)
5. Hanson, D., Challinor, A., Efstathiou, G., Bielewicz, P., Phys, Rev D 83, 043005 (2011)
6. Hirata, C., & Seljak, U., Phys. Rev. D 67, 043001 (2003a)
7. Hirata, C., & Seljak, U., Phys. Rev. D 68, 083002 (2003b)
8. Hu, W., Phys. Rev. D 62, 043007 (2000)
9. Hu, W., ApJ 557: L79-L83 (2001)
10. Hu, W., & Okamoto, T., ApJ 574: 566-574 (2002)
11. Kamionkowski, M., Kosowsky, A., Stebbins, A., Phys. Rev. D 55, 7368-7388 (1997)
12. Kaplinghat, M., Knox, L., Song, Y., Phys. Rev. Lett. 91, 241301 (2003)
13. Kesden, M., Cooray, A., Kamionkowski, M., Phys. Rev. Lett. 89, 011304 (2002)
14. Knox, L., Song, Y., Phys. Rev. Lett. 89, 011303 (2002)
15. Lewis, A. and Challinor, A. and Lasenby, A., ApJ, 538: 473-476 (2000)
16. Okamoto, T., & Hu, W., Phys. Rev. D 67, 083002 (2003)
17. Seljak, U, & Hirata, C., Phys. Rev. D 69, 043005 (2004)
18. Smith, K., Hu W., Manoj, K., Phys. Rev. D 74, 123002 (2006)
19. Zaldarriaga, M., & Seljak, U., Phys. Rev. D 59, 123507 (1999)